iScience, Volume *24*

Supplemental Information

Nitrogen-doped nanoporous graphene induced by a multiple confinement strategy for membrane separation of rare earth

Hongxin Tan, Xin Zhang, Zhan Li, Qing Liang, Jinsheng Wu, Yanli Yuan, Shiwei Cao, Jia Chen, Juewen Liu, and Hongdeng Qiu

TABLE of CONTENTS

TRANSPARENT METHODS

Materials

All reagents and chemicals including Natural graphite powder, amino acids and were purchased from Shanghai Aladdin Industrial Co., Ltd., Shanghai. They were reagent grade and used as received without further purification.

Synthesis of NDNG

A modified Hummers method was used for the preparation of GO from natural graphite powder(Hummers and Offeman 1958). Then the brown GO dispersion (10.0 g/L) was obtained in deionized water via ultrasonic. In a typical process, 0.3 g of phenylalanine (Phe) was dissolved into the 10 mL deionized water, then 10 mL as-prepared aqueous GO dispersion was added. Successively, the mixer of Phe and GO was stirred for approximately 30 min at room temperature. Under vigorous agitation, appropriate amount of $Zn(NO_3)_2$ (1, 2, 3, 4, 6, 8, 9 and 10 g) was added slowly, respectively. The result concentration of $Zn(NO_3)_2$ solution corresponded to 50 g/L, 100 g/L, 150 g/L, 200 g/L, 300 g/L, 400 g/L, 450 g/L and 500 g/L, respectively. Stir evenly, the mixed solution was vacuum filtered by the quantitative filter paper. After drying at 50 °C, all samples of the filter paper with GO, Phe and Zn $(NO_3)_2$ were firstly characterized by XRD with thin film analysis model, then ignited using an alcohol burner. The resulting combustion products were ultrasonicated and centrifuged with diluted HCl and deionized water several times until the eluent was neutral, then dried at 50 °C overnight under vacuum. Here, series of samples are also prepared in a similar method by changing the amount of amino acids (0.2 g, 0.1 g) with concentration of $Zn(NO_3)_2$ 500 g/L. For comparison, Alanine (Ala), no-aromatic amino acid, was used to replace Phe to prepare NDNG in a similar method. Moreover, we also changed the adding order of amino acid and $Zn(NO_3)_2$ to obtain sample of Phe/$Zn(NO_3)_2$/GO, $Zn(NO_3)_2$/Ala/GO, $Zn(NO_3)_2$/Ala/GO and Ala/$Zn(NO_3)_2$/GO, then prepared NDNG for comparing the N-doping content in the final combustion product.

$Zn(NO_3)_2$/Phe/GO: 0.3 g of phenylalanine (Phe) was dissolved into the 10 mL of deionized water, then 10 mL as-prepared aqueous GO dispersion was added. Successively, the mixer of Phe and GO was stirred for approximately 30 min at room temperature. Under vigorous agitation, 10 g of $Zn(NO_3)_2$ was added slowly. Stir evenly, the mixed solution was vacuum filtered by the quantitative filter paper. After drying at 50 °C, the sample was ignited using an alcohol burner. The resulting combustion product was ultrasonicated and centrifuged with diluted HCl and deionized water several times until the eluent was neutral, then dried at 50 °C overnight under vacuum.

Phe/$Zn(NO_3)_2$/GO: Under vigorous agitation, 10 g of $Zn(NO_3)_2$ was added into the 10 mL of deionized water, then 10 mL as-prepared aqueous GO dispersion was added. Then, 0.3 g of phenylalanine (Phe) was dissolved into the above dispersion. Stir evenly, the mixed solution was vacuum filtered directly by the quantitative filter paper. After drying at 50 °C, the sample was ignited using an alcohol burner. The resulting combustion product was ultrasonicated and centrifuged with diluted HCl and deionized water several times until the eluent was neutral, then dried at 50 °C overnight under vacuum.

$Zn(NO_3)_2$/Ala/GO: 0.16 g of alanine (Ala) was dissolved into the 10 mL of deionized water, then 10 mL as-prepared aqueous GO dispersion was added. Successively, the mixer of Ala and GO was stirred for approximately 30 min at room temperature. Under vigorous agitation, 10 g of $Zn(NO_3)_2$ was added slowly. Stir evenly, the mixed solution was vacuum filtered by the quantitative filter paper. After drying at 50 °C, the sample was ignited using an alcohol burner. The resulting combustion product was ultrasonicated and

centrifuged with diluted HCl and deionized water several times until the eluent was neutral, then dried at 50 °C overnight under vacuum.

Ala/$Zn(NO_3)_2$/GO: Under vigorous agitation, 10 g of $Zn(NO_3)_2$ was added into 10 mL of deionized water, then 10 mL as-prepared aqueous GO dispersion was added. Then, 0.16 g of alanine (Ala) was dissolved into the above dispersion. Stir evenly, the mixed solution was vacuum filtered directly by the quantitative filter paper. After drying at 50 °C, the sample was ignited using an alcohol burner. The resulting combustion product was ultrasonicated and centrifuged with diluted HCl and deionized water several times until the eluent was neutral, then dried at 50 °C overnight under vacuum.

Characterizations

All resulting NDNG samples were characterized by transmission electron microscope (TEM, FEI, USA), scanning electron microscope (SEM, HITACHI, Japan), X-ray diffraction (XRD, PANalytical, Netherlands), Raman spectroscopy (HORIBA Jobin Yvon S.A.S., France), and X-ray photoelectron spectroscopy (XPS, ThermoFisher Scientific, USA) equipped with a monochromatic Al Kα X-ray source. Nitrogen adsorption/desorption isotherms were obtained with a Micrometritics ASAP 2020M analyzer (micromeritics, USA) at 77 K, and the specific surface area was calculated from the Brunauer–Emmett–Teller (BET) plot of the N_2 adsorption isotherm. Atomic force microscopy (AFM) images were obtained on a Bruker Dimension Icon (Germany). 5 μL of diluted GO, Phe/GO, and $Zn(NO_3)_2$/Phe/GO aqueous dispersion was dropped on freshly cleaved mica and dried at room temperature to make the AFM samples, respectively.

Separation of REEs

pH Variation Study: 3 mg of NDNG-1 was first prepared by vacuum filter with polyvinylidene fluoride (PVDF) membrane to form membrane for separating of rare earth elements (REEs). The pH of a feed solution of REEs (5mM) was adjusted to 3.0. The pH tests were performed using a driven solution of different concentration of HNO_3 at various pH (1.0, 2.0 and 2.5). The pH was adjusted by diluted NH_4OH or HNO_3 solution.

Effects of membrane thickness: Because of the definite filtration area of 0.79 cm^2, the increasing amount of NDNG certainly increases the thickness of final NDNG membrane. Thus, 2 mg, 3 mg, 4 mg and 5 mg of NDNG-1 were used to prepare membranes with different thickness, respectively. The thickness of the membranes is 45 μm, 105 μm, 157 μm, and 200 μm, respectively. Subsequently, HNO_3 at pH 2 as driven solution and 5 mM of REEs as feed solution were used to perform the permeation and separation of as-obtained membranes.

3 mg of NDNG-1, NDNG-2, NDNG-3, NDNG-4, and NDNG-5, were first prepared to form membranes by vacuum filter for separating of rare earth elements. In the separation tests, the feed solutions containing rare earth ions were prepared with the desired concentration of 5 mM for each element of REEs in a nitric acid environment (pH=3.0). The driven solutions were dilute nitric acid (pH=2.0). As shown in Figure S9K, the feed and driven solutions were put into two independent polytetrafluoroethylene tanks of a made-to-order apparatus, respectively. The NDNG membrane was fixed in the middle of the two tanks with exposed membrane diameter of 1 cm. In order to avoid possible concentration polarization effect near the membrane, magnetic stirring was used both in the feed and permeate solution. In general tests, 5 mL of driven solution after separated for 0.5 h was used to detect elemental quantification of the various elements by inductively coupled plasma mass spectrometry (ICP-MS). The experiments were repeated three times to get standard deviations.

Permeation rate (P) is $\frac{C_t V}{S \times t}$, C_t is the concentration of REEs at a certain time in driven solution, unit is *mol/L*; V is the volume of the driven solution, unit is *L*; S is the effective filter area of NDNG membrane, unit is m^2; t is time, unit is *h*. separation factor $\alpha = \frac{P_1}{P_2}$, p_1 is the permeation rate of the one ion, p_2 is the permeation rate of the other ion.

Computational Methodology

The density functional theory (DFT) calculations were used to calculate the electronic energies. Unconstrained geometry optimizations were performed by the functional B3LYP (Becke, 1993; Lee et al., 1988), with Grimmes DFT-D3 dispersion correction using the Becke-Johnson damping function (Grimme et al., 2011), and the def_2-SVP (Weigend and Ahlrichs, 2005) basis set was adopted. All energies were corrected for the basis set superposition error (BSSE) using the method of Boys and Bernardi (Boys and Bernardi, 1970). All quantum chemistry calculations were performed with Gaussian 16, revision B01 (Thompson and Frechet, 2008). The electrostatic potential (ESP) calculations and (Electron Localization Function) ELF analysis were carried out by using the Multiwfn software package (Revision 3.3.8)(Lu and Chen, 2012), and the isosurface maps were rendered by the VMD 1.9.2 program (Humphrey et al., 1996) based on the outputs of Multiwfn.

Isotherm Adsorption Studies

The pH of all solutions was adjusted to 3, and the REEs concentrations ranging from 0.0031 to 0.125 mM were used to determine the maximum adsorption capacity. Above solutions were kept in a shaker operating at 230 rpm for 24 h to reach the adsorption equilibrium. The concentrations of the remaining REEs were measured by ICP-MS. Adsorption capacity Q_e (mg/g) of NDNG-3 was calculated by the following equation

$$Q_e = (C_i - C_e) \times \frac{V}{M}$$

where C_i (mg/L) and C_e (mg/L) represent initial and equilibrium concentrations of the REEs in solution, respectively. V (L) and M (g) are the volume of the testing solution and the amount of the sorbents NDNG-3, respectively.

SUPPLEMENTAL FIGURES

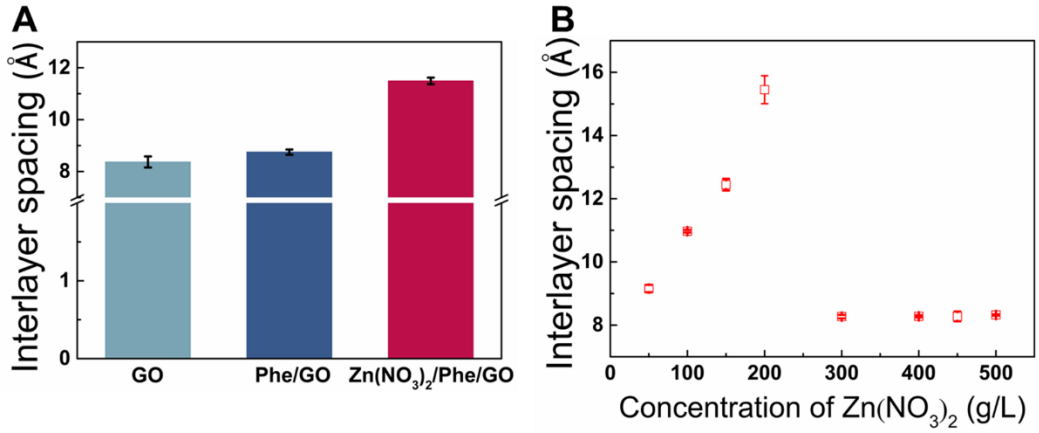

Figure S1. Interlayer spacings of GO composites, related to Figure 1.

(A) Interlayer spacing of GO and GO composites. (B) Interlayer spacing of $Zn(NO_3)_2$/Phe/GO with $Zn(NO_3)_2$ concentration.

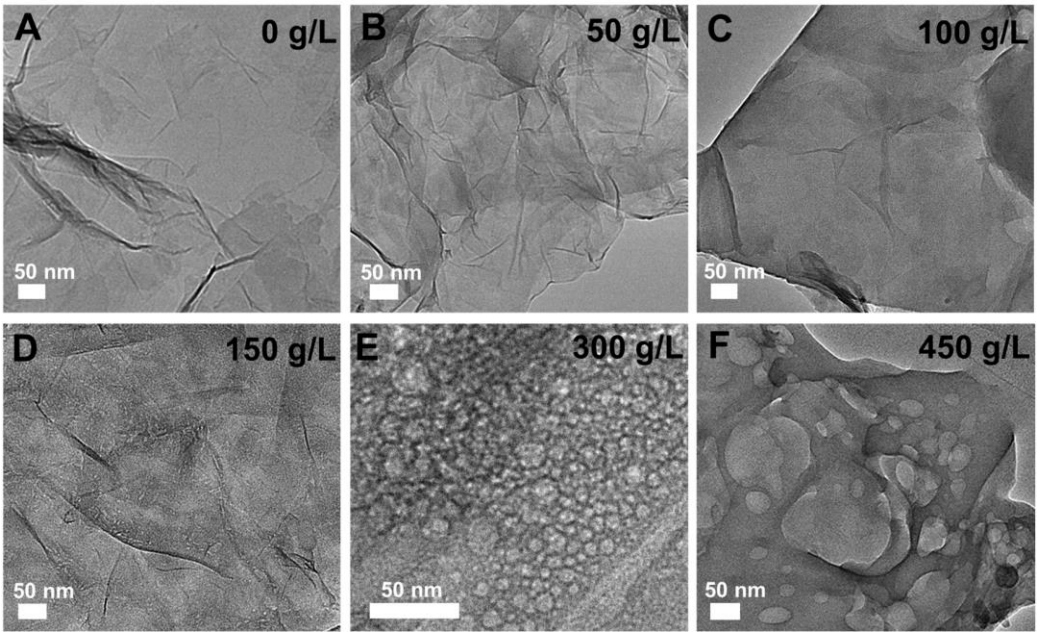

Figure S2. TEM images of the samples $Zn(NO_3)_2$/GO/Phe with different $Zn(NO_3)_2$ concentration, related to Figure 1.

(A) 0 g/L (GO). (B) 50 g/L. (C) 100 g/L. (D) 150 g/L. (E) 300 g/L. (F) 450 g/L.

With the increase of $Zn(NO_3)_2 \bullet 6H_2O$ concentrations, the amount of nitrate crystal water retained between the GO layers gradually increases. When heating and drying after filtration, the larger amount of crystal water from $Zn(NO_3)_2$ can produce the larger volume of vapor bubbles. As these vapor bubbles burst, the larger volume of bubbles would cause the larger size of pores on the surface of hydrotalcite. Therefore, a larger pore of hydrotalcite was observed at higher concentrations of $Zn(NO_3)_2$.

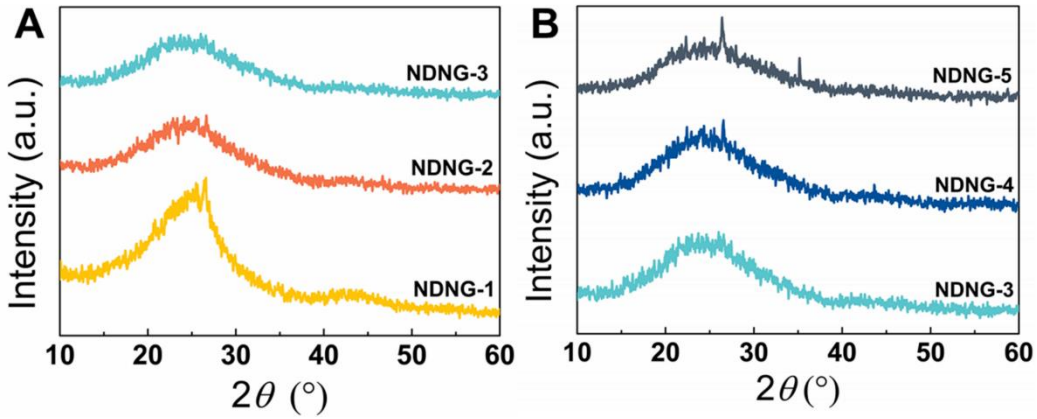

Figure S3. XRD of NDNG, related to Figure 2.

(A) NDNG-1, NDNG-2 and NDNG-3. (B) NDNG-3, NDNG-4 and NDNG-5.

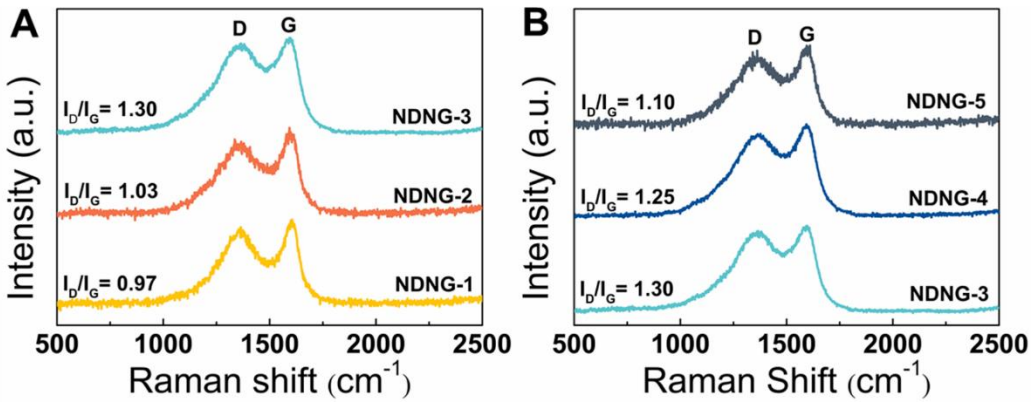

Figure S4. Raman of NDNG, related to Figure 2.

(A) NDNG-1, NDNG-2 and NDNG-3. (B) NDNG-3, NDNG-4 and NDNG-5.

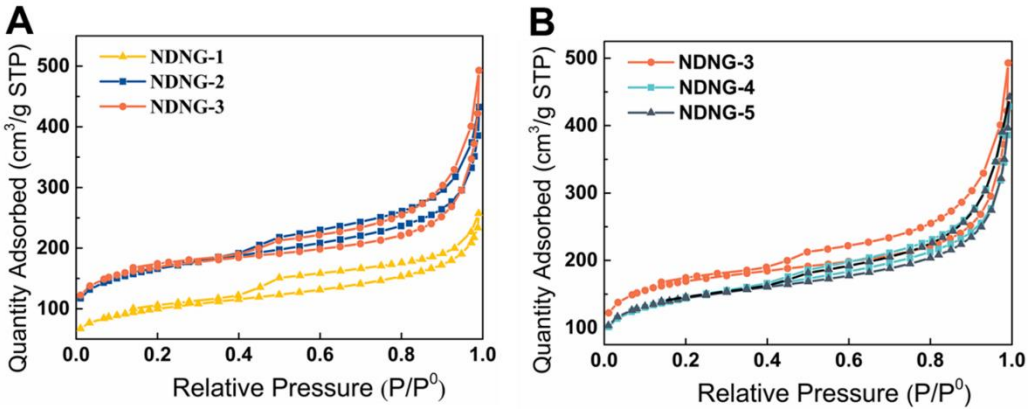

Figure S5. N_2 adsorption−desorption isotherms of NDNG, related to Figure 2.

(A) NDNG-1, NDNG-2 and NDNG-3. (B) NDNG-3, NDNG-4 and NDNG-5.

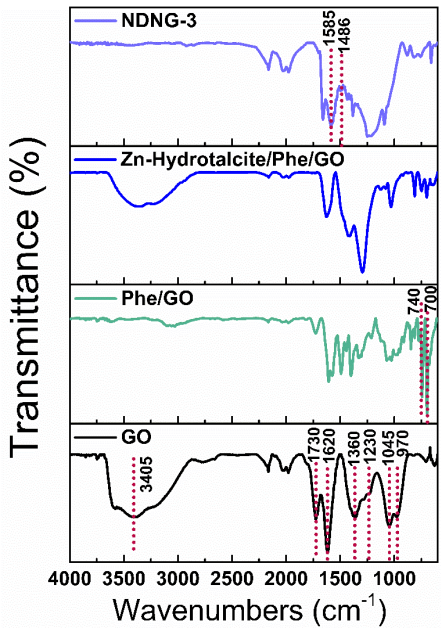

Figure S6. FT-IR spectra of GO, Phe/GO, Zn-hydrotalcite/Phe/GO and NDNG-3 samples, related to Figure 2.

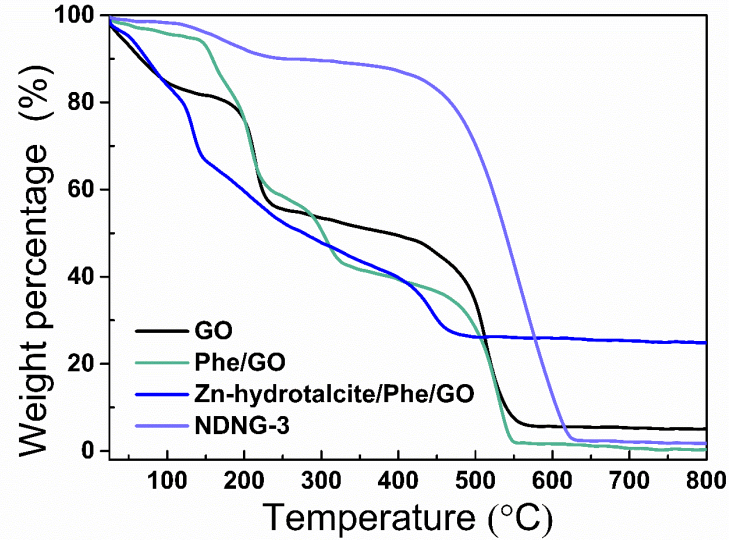

Figure S7. TGA curves of GO, Phe/GO, Zn-hydrotalcite/Phe/GO and NDNG-3 samples under air atmosphere, related to Figure 2.

The chemical structures of the GO, Phe/GO, Zn-hydrotalcite/Phe/GO, and NDNG-3 samples were characterized to monitor the synthetic processes by Fourier transform infrared (FT-IR) (Figure S6). As shown in Figure S6, there are many O-containing groups that exist on GO sheets. The characteristic functional groups of GO were observed at 3405 cm^{-1} (C-OH), 1730 cm^{-1} (C=O), 1620 cm^{-1} (C=C), 1360 cm^{-1} (C–OH), 1230 cm^{-1}, 1045 cm^{-1} and 970 (C–O) cm^{-1}, respectively. Compared with that of pure GO, the FT-IR spectrum of Phe/GO showed several differences from that of GO, such as the peaks at 740 and 700 cm^{-1} associating with Phe. The result suggests that after mixing with GO, Phe was successfully adsorbed by GO. After the formation of the Zn-hydrotalcite on the Phe/GO sheets, some prominent peaks shifted largely or disappeared, which was due to strongly interactions between Zn-hydrotalcite and functional groups on the Phe/GO sheets. It should be noted that the peak at 1730 cm^{-1} of GO disappeared and new absorption peaks at 1486 cm^{-1} and 1585 cm^{-1} corresponding to C-N and C=N stretching appeared, indicating that most of the O-containing groups were removed and NDNG was successfully prepared.

In order to understand the observations, thermogravimetric analysis (TGA) tests were carried out on several samples (Figure S7). TGA of the GO has a mass loss before 100 °C due to the removal of trapped water between the sheets of GO. The mass removal in the range 200–230 °C was attributed to the decomposition of less stable oxygen functionalities. Between 230 and 800 °C, a gradual weight loss was observed and can be related to the removal of more stable oxygen functionalities and graphitic regions. It is worth noting that the presence of Phe and Zn-hydrotalcite in the samples of Phe/GO and Zn-hydrotalcite/Phe/GO remarkably changes the thermal process of GO, suggesting that the structure of Zn-hydrotalcite/Phe/GO was successfully prepared.

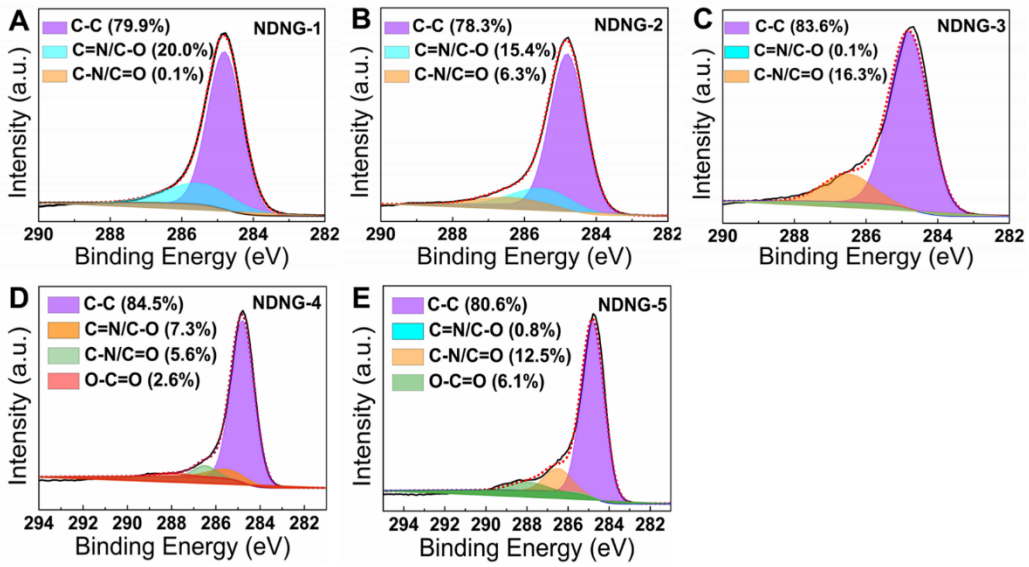

Figure S8. Typical high resolution XPS C 1s spectra of the NDNG, related to Figure 3.

(A) NDNG-1. (B) NDNG-2. (C) NDNG-3. (D) NDNG-4. (E) NDNG-5.

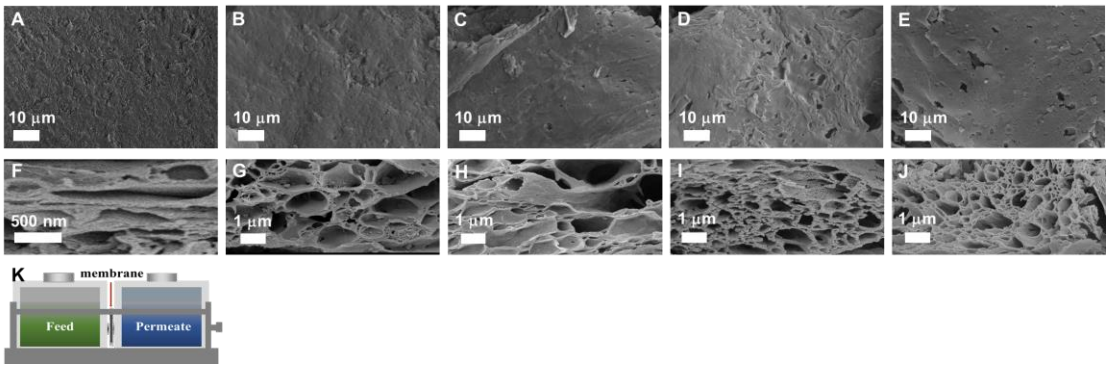

Figure S9. SEM images of surface and cross-section of NDNG membranes, related to Figure 4.

(A-E) SEM image of the surface morphology of NDNG membranes prepared with NDNG-1 (A), NDNG-2 (B), NDNG-3 (C), NDNG-4 (D), and NDNG-5 (E). (F-J) SEM image of the cross-sectional view of NDNG membranes prepared with NDNG-1 (F), NDNG-2 (G), NDNG-3 (H), NDNG-4 (I), and NDNG-5 (J). (K) schematic of ion separation equipment, REEs solution and HNO_3 solution are placed as the feed and permeate solutions, respectively.

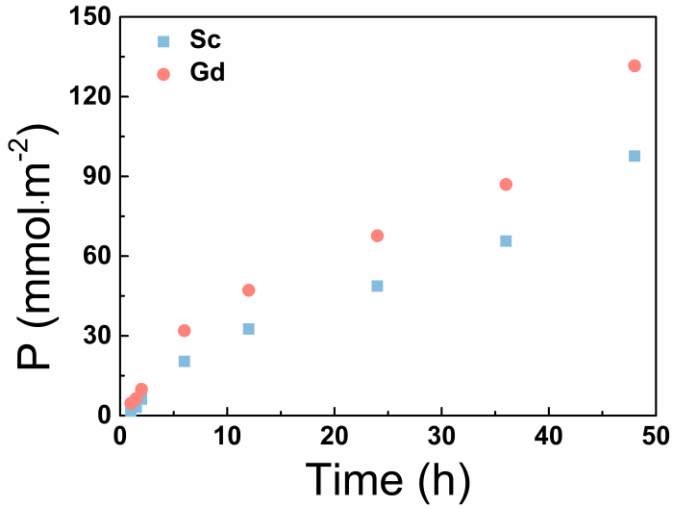

Figure S10. Kinetic study of Sc^{3+} and Gd^{3+} separation through NDNG-1 membrane, related to Figure 4.

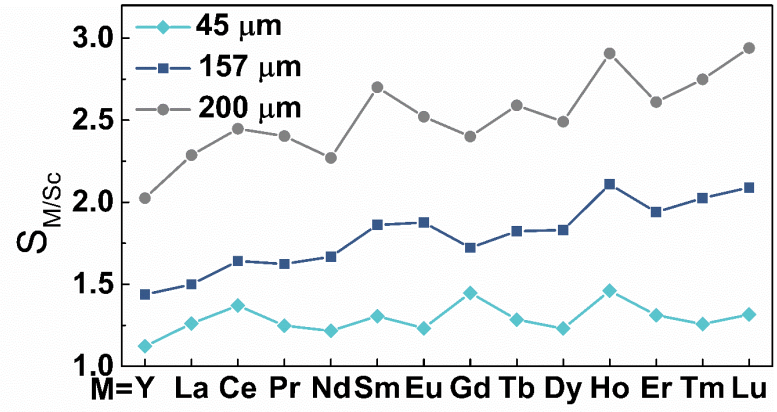

Figure S11. Separation factor of REEs as a function of the NDNG-1 membrane thickness, related to Figure 4.

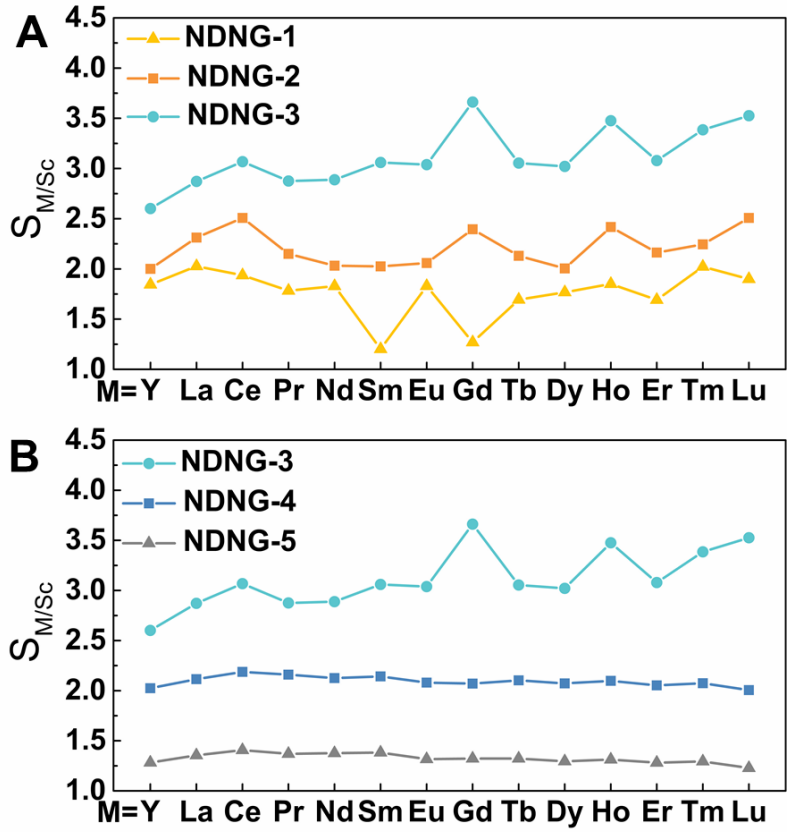

Figure S12. Separation factor with different NDNG membranes of M/Sc (M = Y, La, Ce, Pr, Nd, Sm, Eu, Gd, Tb, Dy, Ho, Er, Tm, Lu.), related to Figure 4.

(A) NDNG-1, NDNG-2, NDNG-3. (B) NDNG-3, NDNG-4, and NDNG-5. The feed solution has a concentration of 5 mM for all elements at a pH of 3.0; The driven solution is dilute nitric acid at a pH of 2.0.

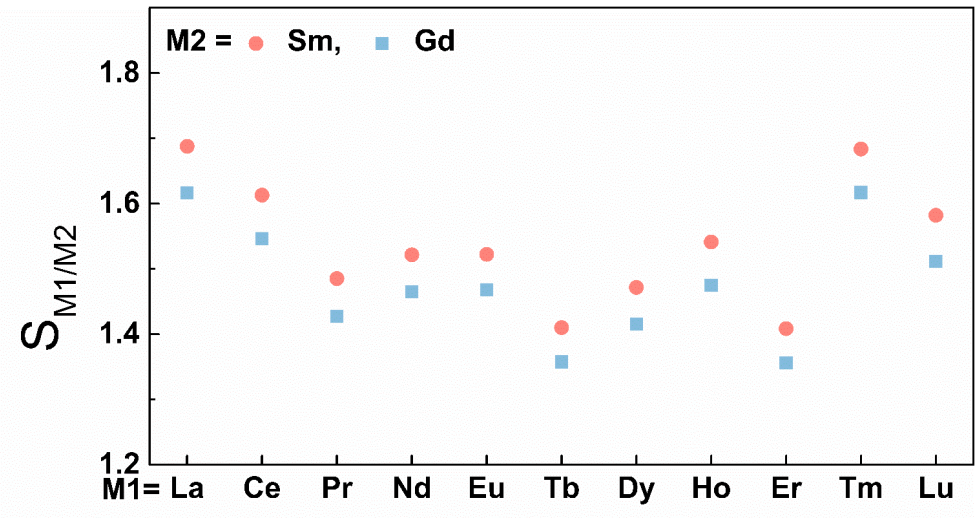

Figure S13. Selective separation of lanthanide M_2 (Sm and Gd) and other lanthanide M_1 for NDNG-3 membrane, related to Figure 4.

M_1 is selected from the lanthanide elements except Sm and Gd, and M_2 is chosen from Sm and Gd.

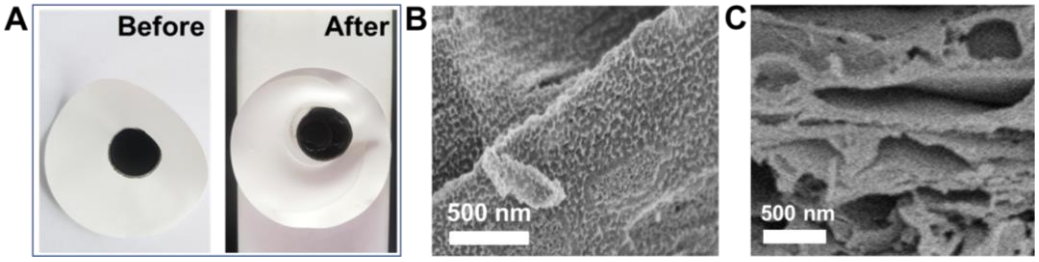

Figure S14. stability of NDNG membrane in acidic (pH = 3.0) solutions after 90 days, related to Figure 4.

(A) Photos of a NDNG membrane before and after separation of REEs. SEM images of surface (B) and cross-section (C) of NDNG membrane prepared with NDNG-1 after separation of REEs.

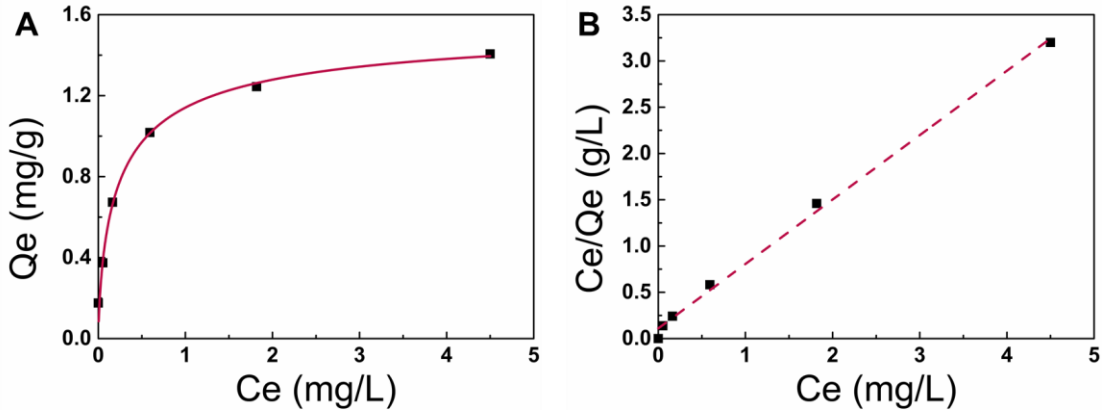

Figure S15. Experimental equilibrium isotherm data and modeling for Sc^{3+} sorption on NDNG-3, related to Figure 5.

(A) Equilibrium isotherms for the adsorption of Sc^{3+} in the presence of other REEs by NDNG-3, pH = 3, m = 4 mg, V= 5 mL. (B) Fitting for the Langmuir model.

SUPPLEMENTAL TABLES

Table S1. Atomic Composition of NDNG and Nanoporous Graphene, related to Figure 3

Sample	C %	N %	O %
$Zn(NO_3)_2$/Phe/GO	78.6	2.5	17.0
Phe/$Zn(NO_3)_2$/ GO	85.4	1.9	11.1
$Zn(NO_3)_2$/Ala/GO	80.0	0.9	16.6
Ala/$Zn(NO_3)_2$/ GO	82.1	0.8	15.0
$Zn(NO_3)_2$/ GO	83.2	0.0	14.2

All samples were performed in triplicates, and only the average is presented.

As shown in Table S1, the nitrogen element cannot be detected in the product of the sample $Zn(NO_3)_2$/GO (nanoporous graphene).

Table S2. Comparison of Separation Factor with Ion Imprinted Membranes, related to Figure 4

No.	Target ion	Interfering ion	Separation Factor	Ref.
1	Eu^{3+}	La^{3+}, Gd^{3+}, Sm^{3+}	3.82, 3.47, 3.34	[Chen et al., 2018)]
2	Gd^{3+}	La^{3+}, Ce^{3+}	3.50, 2.23	[Li et al., 2015]
3	Ce^{3+}	Fe^{3+}	3.2	[Liu et al., 2014]
4	Gd^{3+}	La^{3+}, Eu^{3+}	2.91, 2.49	[Cui et al., 2019]
5	Nd^{3+}, Dy^{3+}	Pr^{3+}, Tb^{3+}	3.02, 4.16	[Zheng et al., 2018]
6	Nd^{3+}	Pr^{3+}	3.56	[Zheng et al., 2017]
7	Dy^{3+}	Nd^{3+}	3.33	[Liu et al., 2017]
8	Sc^{3+}	Other REEs	3.7	This work

Table S3. Langmuir Model Parameter Calculated from Adsorption Isotherm, related to Figure 5

Sample	K_L (L/mg)	Q_m (mg/g)	R^2
NDNG-3	6.2823	1.4369	0.9958

SUPPLEMENTAL REFERENCES

Becke, A.D. (1993). DENSITY-FUNCTIONAL THERMOCHEMISTRY .3. THE ROLE OF EXACT EXCHANGE. J. Chem. Phys. *98*, 5648-5652.

Boys, S.F., and Bernardi, F. (1970). CALCULATION OF SMALL MOLECULAR INTERACTIONS BY DIFFERENCES OF SEPARATE TOTAL ENERGIES-SOME PROCEDURES WITH REDUCED ERRORS. Mol. Phys. *19*, 553-566.

Grimme, S., Ehrlich, S., and Goerigk, L. (2011). Effect of the Damping Function in Dispersion Corrected Density Functional Theory. J. Comput. Chem. *32*, 1456-1465.

Hummers, W.S., Offeman, R.E., 1958. PREPARATION OF GRAPHITIC OXIDE. J. Am. Chem. Soc. *80*, 1339-1339.

Humphrey, W., Dalke, A., and Schulten, K. (1996). VMD: Visual molecular dynamics. J. Mol. Graphics Modell. *14*, 33-38.

Lee, C.T., Yang, W.T., and Parr, R.G. (1988). DEVELOPMENT OF THE COLLE-SALVETTI CORRELATION-ENERGY FORMULA INTO A FUNCTIONAL OF THE ELECTRON-DENSITY. Physical Review B *37*, 785-789.

Lu, T., and Chen, F. (2012). Multiwfn: A multifunctional wavefunction analyzer. J. Comput. Chem. *33*, 580-592.

Thompson, B.C., and Frechet, J.M.J. (2008). Organic photovoltaics-Polymer-fullerene composite solar cells. Angew. Chem., Int. Ed. *47*, 58-77.

Weigend, F., and Ahlrichs, R. (2005). Balanced basis sets of split valence, triple zeta valence and quadruple zeta valence quality for H to Rn: Design and assessment of accuracy. Phys. Chem. Chem. Phys. *7*, 3297-3305.